

1   **Sphingomyelin biosynthesis is critical in organizing phosphoinositide turnover during  
2   phagocytic uptake of *Mycobacterium tuberculosis***

3   *Patrick Niekamp<sup>\*1,2</sup>, Gaelen Guzman<sup>\*1</sup>, Hans Leier<sup>1</sup>, Ali Rashidfarrokhi<sup>3</sup>, Veronica Richina<sup>4</sup>,*  
4   *Fabian Pott<sup>1</sup>, Joost CM Holthuis<sup>2</sup>, Fikadu G. Tafesse<sup>1#</sup>*

5

6   \*These authors contributed equally.

7   <sup>1</sup>Department of Molecular Microbiology and Immunology, Oregon Health & Science University,  
8   3181 SW Sam Jackson Park Road, Portland, OR 97239.

9   <sup>2</sup>Biology & Chemistry Department, University of Osnabrück, Fachbereich Biologie/Chemie,  
10   Barbarastrasse 13, 49076 Osnabrück, GERMANY. <sup>3</sup>Department of Pathology and Department of  
11   Medicine, New York University Langone, 550 First Avenue, MSB 594, New York, NY 10016.

12   <sup>4</sup>Department of Biomedicine University Basel Hebelstrasse 20 4031 Basel Switzerland.

13

14   #Correspondence: tafesse@ohsu.edu

15

16    **Abstract**

17    Phagocytosis by alveolar macrophages is the obligate first step of infection by *Mycobacterium*  
18    *tuberculosis*, yet the mechanisms of this potential vulnerability in the bacterial life cycle are  
19    incompletely understood. Here we show that sphingolipids, a lipid class enriched in the outer  
20    leaflet of plasma membranes, are required for *M. tuberculosis* to efficiently enter and infect  
21    phagocytes. Genetic knockout or inhibition of serine palmitoyltransferase or ceramide synthases,  
22    key enzymes that catalyze the *de novo* sphingolipid biosynthesis, greatly reduces *M. tuberculosis*  
23    uptake by diverse phagocytic cell types without affecting other forms of endocytosis. This  
24    phenotype is caused by multiple defects in the cellular processes that are critical for the  
25    formation of a phagocytic cup. While the clustering of innate immune receptors such as Dectin-1  
26    is normal, the exclusion of the regulatory phosphatase CD45 from the receptor engagement site  
27    at the phagocytic synapse is defective in cells deficient in sphingolipid biosynthesis. We also  
28    show that the turnover of phosphoinositides and activation of small GTPases at the phagosomal  
29    synapse are impaired upon blockade of sphingolipid synthesis. Human monocytes deficient in  
30    sphingomyelin biosynthesis show reduced *M. tuberculosis* uptake comparable to that of cells  
31    depleted of total sphingolipids, indicating that sphingomyelin is specifically required for  
32    phagocytosis. Together, these data identify the sphingomyelin biosynthetic pathway as a critical  
33    cellular process mediating the earliest stage of *M. tuberculosis* invasion and establish the  
34    significance of this lipid in innate immune responses.

35

36 **Introduction**

37         The etiologic agent behind an estimated 10 million new cases of tuberculosis and 1.6  
38 million deaths in 2017 alone, *Mycobacterium tuberculosis* (Mtb) has established itself as a highly  
39 effective and insidious pathogen<sup>1,2</sup>. Mtb invades alveolar immune cells through phagocytosis, and  
40 wields an extensive repertoire of effector molecules that operate to dampen the immune response,  
41 reprogram the host lipidome, and promote long-term intracellular survival<sup>3,4</sup>. As an intracellular  
42 pathogen, Mtb necessarily interacts with its host along numerous lipid interfaces throughout its  
43 infectious lifecycle. Understanding the biological roles of host lipids during infection may  
44 illuminate novel routes of therapeutic strategies to prevent the onset and spread of tuberculosis<sup>5</sup>.

45         In most settings, phagocytosis is critical for clearing dead and effete cells, and serves  
46 as a first line of defense against microbial pathogens. This process culminates in the  
47 engulfment and internalization of target particles, which are subsequently degraded following  
48 convergence of the phagosome with the lysosome<sup>6</sup>. In the context of pathogen clearance, uptake  
49 by professional phagocytes (primarily monocytes, macrophages, and dendritic cells) results in a  
50 robust inflammatory response and antigen presentation that may contribute to an adaptive immune  
51 response<sup>7</sup>. For example, previous work shows that phagocytic uptake of *Candida albicans* is  
52 essential for the clearance of infection *in vivo*<sup>8</sup>. In contrast, Mtb is highly adept at subverting its  
53 own degradation to survive within phagosome-derived compartments through an array of  
54 mechanisms. As one example, this pathogen inhibits the Ca<sup>2+</sup>-dependent fusion of the phagosome  
55 to the lysosome by disrupting the activity of sphingosine kinase<sup>6,9</sup>. Cholesterol is reported to be  
56 required for Mtb entry<sup>10</sup>. Despite extensive literature on the host-pathogen interactions of Mtb, the  
57 specific functional roles played by host lipid species at the site of initial phagocytic  
58 uptake of Mtb have remained relatively unstudied. In particular, structural and signaling functions

59 played by sphingolipids at the cell membrane and within the phagosome during Mtb infection are  
60 unknown.

61 Sphingolipids are a complex family of membrane lipids that contain a sphingoid base. A  
62 species of particular note, sphingomyelin constitutes a significant fraction of the total lipid  
63 composition of the exoplasmic leaflet of the plasma membrane and plays critical roles in the  
64 organizing membrane dynamics at the cell surface<sup>11,12</sup>. A growing body of literature shows that  
65 sphingolipids mediate functions beyond existing as membrane barrier components: members of  
66 this family accumulate in specialized lipid domains and act as secondary messengers within the  
67 cell<sup>13–15</sup>. These signaling functions are relevant to many biological processes that span  
68 from apoptosis and autophagy to stress response and inflammation in many (if not all) mammalian  
69 cell types<sup>16–18</sup>. The cellular proportions of ceramide and sphingosine-1-phosphate have been shown  
70 to act as a rheostat that determines cell survival under stress<sup>19</sup>. Notably, it has been shown that the  
71 biosynthetic flow of sphingolipids through the Golgi creates a regulatory feedback loop that  
72 controls the levels of phosphatidylinositol-4-phosphate, although interactions outside of the *trans*-  
73 Golgi network are unknown<sup>20</sup>.

74 Prior work has investigated the roles played by sphingolipids during the phagocytosis of  
75 other particles – contradictory reports describe the effect of sphingolipid depletion during  
76 phagocytosis. We have previously reported that cellular sphingolipids are critical for the *in vivo*  
77 clearance of *Candida albicans* infection through phagocytosis by macrophages<sup>8</sup>. In contrast,  
78 depletion of cellular sphingolipids reportedly enhances phagocytic uptake of opsonized particles<sup>21</sup>.  
79 Together, these results suggest that the roles played by sphingolipids during phagocytosis may be  
80 pathogen or particle specific, based on the specific ligands decorating a particle<sup>22</sup>. However, the  
81 role of sphingolipids during entry of Mtb remained poorly understood.

82           Here, we employed chemical and genetic tools to manipulate levels of sphingolipids in  
83           mammalian phagocytes, and infected them using an mCherry-expressing reporter strain of H37Rv  
84           Mtb. We first show that host sphingolipid depletion reduces the capacity of Mtb to invade host  
85           cells through phagocytosis – but that other mechanisms of endocytosis are unaffected. We next  
86           show that sphingolipid depletion resulted in the impairment of the regulatory phosphatase CD45  
87           displacement by phagocytic receptors at the site of particle engagement. Furthermore, we  
88           demonstrate that blockade of sphingolipid biosynthesis results in defects of phagocytic signaling,  
89           including an unsuccessful activation and recruitment of the small GTPases Rac1 and CD42 to the  
90           phagocytic cup. This in turn resulted in only transient and futile turnover of phosphoinositidyl-4,5-  
91           bisphosphate, a critical process for actin remodeling during phagosome formation. Finally, we  
92           show that specifically inhibiting the *de novo* synthesis of sphingomyelin results in a robust  
93           phenocopy of total blockade of sphingolipid biosynthesis. Together, these data demonstrate that  
94           intact sphingomyelin biosynthesis is required for the earliest stages of *M. tuberculosis* invasion  
95           and highlights the importance of this host lipid in innate immune responses against this pathogen.

96

97 **Results**

98 **Manipulating sphingolipid biosynthesis in mammalian phagocytes using genetic and  
99 chemical tools**

100 To define the role of the sphingolipid biosynthetic pathway in phagocytic uptake of Mtb,  
101 we sought to inhibit sphingolipid biosynthesis in four different phagocytic cell lines: the murine  
102 macrophage cell line RAW 246.7, the murine dendritic cell line DC2.4, the human monocyte cell  
103 lines THP-1 and U937. We first used a chemical approach to inhibition using the compounds  
104 myriocin (Myr) and fumonisin B1 (FB1). As depicted in Figure 1A, the initial and rate limiting  
105 step of sphingolipid synthesis is the production of the sphingoid base through the condensation of  
106 serine and palmitoyl-CoA, and is performed by the enzymatic complex serine palmitoyltransferase  
107 (SPT)<sup>23</sup>. Previously we reported that genetic ablation of Sptlc2 results in blockade of *de novo*  
108 synthesis of all sphingolipid, as does treatment with the atypical amino acid Myr<sup>8</sup>. The fungal toxin  
109 FB1 acts several steps downstream in the sphingolipid biosynthetic pathway by blocking the  
110 activity of ceramide synthase<sup>8</sup>. As the central nexus of sphingolipid synthesis, ceramide is  
111 converted into many classes of higher sphingolipids - including sphingomyelin,  
112 glycosphingolipids, and galactosylceramides<sup>19,24</sup>.

113 To verify the reported effects of myriocin and fumonisin B1 and Sptlc2 knockout, we used  
114 thin layer chromatography to visualize the incorporation of 3-L-[<sup>14</sup>C]-serine into sphingolipid  
115 species in RAW 246.7, THP-1, DC2.4, and U937 cells following 3-day treatment with Myr and  
116 FB1 (Figure 1B and D and Supplementary Figure 1). Across all cell lines, treatment with these  
117 compounds resulted in significant reduction of sphingolipid content, without disrupting  
118 phosphatidylserine content – demonstrating the specificity and potency of these compounds  
119 (Figure 1E and F).

120 To further examine the lipid composition of cells deficient in sphingolipid biosynthesis,  
121 we performed mass spectrometry-based lipidomic analysis of RAW 264.7 macrophages following  
122 treatment with chemical inhibitors and Sptlc2 knockout. We examined cellular levels of  
123 sphingosine, ceramide, sphingomyelin, and glucosylceramide. As expected, both myriocin and  
124 Sptlc2 knockout result in significant reduction of all sphingolipid species (Figure 1 G-J). In FB1  
125 treated cells, we observe reduction of all sphingolipid species downstream of ceramide synthesis  
126 (the point of inhibition along the biosynthetic pathway), but we observe a concordant increase in  
127 sphingosine (synthesized upstream of ceramide), as previously reported (Figure 1G-J)<sup>25</sup>.  
128 We then sought to verify the mutation in Sptllc2 gene or inhibitor treatments do not have a  
129 pleiotropic effect. To this end, we carefully examined for any defect in the overall viability and  
130 morphology of the cell. Despite a reduced level of sphingolipids, these cells grow normally with  
131 no apparent defect in morphology or viability (Supplementary Figure 2). Notably, we observe  
132 that myriocin and FB1 treatment, as well as Sptlc2 knockout, do not result in the total ablation of  
133 cellular sphingolipid content. This is at least partially attributable to the activity of the  
134 sphingolipid salvage pathways, through which cells may acquire sphingolipids from additives in  
135 media – primarily serum. It is likely that cells deficient in sphingolipid biosynthesis acquire  
136 sphingolipids from media at only the minimal level to allow cell growth, as their overall  
137 sphingolipid content is significantly lower than in wildtype cells (Figure 1D-J). This is consistent  
138 with our previous report that shows the Sptlc2<sup>-/-</sup> DC2.4 cells do not harbor any significant defect  
139 with regards to cell survival, morphology, and membrane trafficking<sup>8</sup>. As described below, the when  
140 grown in the presence of serum, the primary phenotype following blockade of sphingolipid  
141 biosynthesis is a reduced rate of phagocytic uptake of pathogens such as Mtb.  
142

143 **Cells deficient in sphingolipid biosynthesis display reduced capacity to phagocytose Mtb.**

144 To investigate the role of sphingolipids during phagocytic uptake of Mtb, we used Myr and  
145 FB1 to block sphingolipid synthesis in RAW 264.7, THP-1, DC2.4, and U937 cells. We then  
146 infected cells with an mCherry-expressing strain of Mtb to quantify rates of phagocytosis. Figure  
147 2A depicts the experimental and analysis workflow. Briefly, cells were infected at a multiplicity  
148 of infection (MOI) of 10 for two hours, after which cells were fixed and stained with DyLight 488-  
149 conjugated phalloidin and with DAPI (to visualize F-actin at cell boundary and nuclei,  
150 respectively). Fluorescence microscopy was used to quantify uptake efficiency through automated  
151 counting of cell number (by nuclei) and internalized bacteria (red fluorescent particles within green  
152 cell boundary). We report uptake efficiency as the ratio of the total number of internalized Mtb  
153 particles against the number of identified nuclei, and normalized the uptake rate of treated cells to  
154 that of untreated cells to address variability between biological replicates. In all cell models  
155 analyzed, we observed a statistically significant reduction in Mtb uptake of approximately 50%  
156 following treatment with myriocin, and approximately 40% for FB1 (Figure 2B-I). Similarly, the  
157 knockout of Sptlc2 resulted in approximately 50% of wildtype uptake in both RAW 264.7 and  
158 DC2.4 cells (Figure 3A-D). These results suggest that the maintenance of total cellular  
159 sphingolipid levels through active sphingolipid biosynthesis is required for efficient phagocytic  
160 uptake of Mtb across four model cell lines and irrespective of the mechanism of inhibition.

161 We next sought to assess whether blocking sphingolipid biosynthesis affects the  
162 phagocytosis of Zymosan A, a model particle composed of  $\beta$ -glucan chains derived from  
163 *Saccharomyces cerevisiae*. Zymosan A particles engage the C-type Lectin receptor Dectin-1,  
164 expressed on professional phagocytes<sup>8,26,27</sup>. Dectin-1 is one of several pathogen recognition  
165 receptors that engage Mtb and initiate phagocytic signaling to facilitate host cell entry<sup>28,29</sup>. We

166 thus hypothesized that inhibiting sphingolipid biosynthesis in host cells would result in a reduced  
167 uptake rate for this Zymosan A, reflecting that of Mtb. We found that Sptlc2-deficient RAW 264.7  
168 cells are reduced in their capacity to uptake Zymosan A to a similar degree as to that of Mtb uptake  
169 (Figure 3E and F). We thus used Zymosan A as a model particulate to gain further insight regarding  
170 the mechanism in which sphingolipids are involved in phagocytosis.

171 **Sphingolipid-depleted cells are permissive to virus that utilizes phagocytosis-like cellular  
172 processes.**

173 Are the effects of sphingolipid depletion restricted to phagocytic uptake? To answer this  
174 question, we performed parallel infections of RAW 264.7 wildtype and Sptlc2 knockout cells using  
175 a fluorescent reporter strain of Herpes Simplex Virus-1 (HSV) encoding a fusion of viral protein  
176 VP26 and mCherry<sup>30</sup>. HSV is an enveloped virus that gains entry to host cells through the  
177 phagocytosis-like process of macropinocytosis, and the viral receptors have been shown to be  
178 nectin-1 (also known as herpesviruses entry mediator)<sup>31,32</sup>. It has been shown that HSV entry is  
179 dependent on cholesterol and dynamin2<sup>33</sup>. At 12-hours post-infection, we visualized and quantified  
180 rates of infection using high-content imaging as described above. Because the VP26-mCherry  
181 reporter construct localizes to the nucleus, we did not stain cells using phalloidin and instead used  
182 the co-localization of DAPI with mCherry as a measure of infection. We observe that there is no  
183 significant difference in the infection rates of wildtype and Sptlc2<sup>-/-</sup> cells, suggesting that  
184 sphingolipids play no significant role in the entry of HSV-1 (Figure 3G and H). These data  
185 demonstrate that endocytic pathways are functional in sphingolipid-deficient cells, suggesting a  
186 specific role for sphingolipids in phagocytosis of bacterial pathogens such as Mtb by immune  
187 cells.

188

189     **The exclusion of the regulatory phosphatase CD45 from the site of particle engagement is  
190     impaired in Sptlc2<sup>-/-</sup> cells**

191         It has been shown that the engagement of phagocytic receptor to ligand initiates the  
192         accumulation of pathogen recognition receptors to the phagocytic synapse, which results in the  
193         physical expulsion of inhibitory phosphatases such as CD45 from the phagocytic synapse and the  
194         formation of a lipid raft-like domain<sup>34</sup>. Prior work has shown that the several intracellular  
195         pathogens, including Mtb, induce their uptake in a cholesterol-dependent manner<sup>5,35</sup>. Because  
196         sphingolipids such as sphingomyelin have been shown to play a role in the formation of both lipid  
197         raft and cholesterol-rich domains, we hypothesized that cellular sphingolipid content is required  
198         for the aggregation of the pathogen recognition receptor Dectin-1 to the site of particle  
199         engagement, and the concomitant exclusion of CD45 from the contact site.

200         To address this hypothesis, we transiently transfected wildtype and Sptlc2<sup>-/-</sup> RAW 264.7  
201         macrophages with a GFP-tagged Dectin-1 construct, and assessed the co-localization of this  
202         fluorescent protein with the inhibitory phosphatase CD45 upon treatment with non-fluorescent  
203         Zymosan A particles two minutes post-incubation. In both wildtype and Sptlc2 knockouts, we find  
204         that Dectin-1 aggregates at the site of contact with Zymosan A within the first two minutes. As  
205         expected, in wildtype cells the inhibitory phosphatase CD45 is efficiently displaced by Dectin-1.  
206         To this end, the co-localization of CD45 with Dectin-1 in wildtype cells is significantly reduced at  
207         the site of particle engagement (Figure 4A and B). In contrast, the co-localization of Dectin-1-GFP  
208         and CD45 in Sptlc2 knockout cells is only minimally reduced (Figure 4A and B). These data  
209         suggest that sphingolipid biosynthesis is required to mediate the proper displacement of CD45, a  
210         step that is critical for the initiation of phagocytic synapse formation.

211 To control against the possibility that deficient sphingolipid biosynthesis results in altered  
212 surface expression of CD45 and Dectin-1, we used flow cytometry to compare surface expression  
213 of these proteins between wildtype and Sptlc2<sup>-/-</sup> RAW 264.7 cells. We probed cells for endogenous  
214 surface protein using APC-conjugated anti-CD45 antibody and FITC-conjugated anti-Dectin-1  
215 antibody. We found agreement in overall fluorescent signal for both wildtype and Sptlc2 knockout  
216 cells for both surface markers (Figure 4C-F). These results suggest that the levels of both CD45  
217 and Dectin-1 at the cell surface are unaffected by blocking the biosynthesis of sphingolipids.

218

219 **Activation of Rho GTPases Rac1 and Cdc42 are defective in Sptlc2<sup>-/-</sup> cells.**

220 As we describe above, the initial stages of phagosomal synapse formation are impaired in  
221 Sptlc2<sup>-/-</sup> cells. Downstream of receptor activation, phagocytosis is strictly regulated through a  
222 signaling network that involves the dynamic activation and recruitment of both enzymes (such as  
223 GTPases, kinases, and phosphatases) and lipids – particularly several phosphatidylinositol species.  
224 To determine whether blocking sphingolipid biosynthesis perturbs downstream phagocytic  
225 signaling events following particle engagement, we transfected wildtype and Sptlc2<sup>-/-</sup> cells with  
226 Rac1/Cdc42 fluorescent biosensors to examine the activation and localization of these proteins  
227 during phagocytosis.

228 As depicted in Figure 5A, the Rho GTPases Rac1 and Cdc42 are activated via  
229 phosphorylation following engagement of phagocytic receptors to pathogenic particles such as  
230 Mtb<sup>36</sup>. To visualize the activation of these GTPases, we transfected wildtype and Sptlc2<sup>-/-</sup> RAW  
231 264.7 macrophages with a fluorescent biosensor consisting of the fusion of YFP to the p21-binding  
232 domain of the p21-activated kinase (PBD(PAK)-YFP) – this biosensor enables the visualization  
233 of localized GTPase activation<sup>37,38</sup>. Twenty-four hours after transfection, we infected cells using

234 Zymosan A particles at an MOI of 10 and performed live imaging to visualize the distribution of  
235 PBD(PAK)-YFP in these cells. In wildtype cells, we observe increased localization of fluorescent  
236 signal to the site of particle contact – corresponding to the expected pattern of Rac1/Cdc42  
237 activation (Figure 5B and C, and Supplementary Movie1). In Sptlc2<sup>-/-</sup> cells on the other hand, we  
238 observed only a transient (and futile) activation which resulted in significantly reduced  
239 accumulation of a sustained fluorescent signal in Sptlc2<sup>-/-</sup> cells, suggesting that these cells are  
240 defective in the activation of Rho GTPases following particle binding (Figure 5B and C, and  
241 Supplementary Movie2).

242

### 243 **Phosphatidylinositol turnover is impaired in Sptlc2 knockout cells.**

244 Next, we visualized the turnover of phosphatidylinositols at the phagocytic synapse. Rho  
245 GTPase activation initiates the conversion of phosphatidylinositol-4-phosphate (PIP) to  
246 phosphatidylinositol-4,5-bisphosphate (PIP2) at the base of the phagocytic synapse. The  
247 accumulation of PIP2 is essential to initiate the polymerization of actin filaments that drive the  
248 leading edges of the growing phagosome around the particle<sup>38</sup>. Following the leading edge of PIP2  
249 production, the enzyme phosphatidylinositol 3-kinase (PI3K) converts PIP2 into  
250 phosphatidylinositol-3,4,5-trisphosphate (PIP3), which initiates a trailing edge of actin  
251 disassembly at the base of the phagosomal cup (Figure 5A)<sup>7</sup>. To date, there have been no reports  
252 connecting phosphoinositide signaling to cellular sphingolipid biosynthesis during phagocytosis.  
253 However, sphingolipid and phosphoinositide levels within the Golgi regulate each other in a  
254 homeostatic feedback circuit: buildup of sphingomyelin in the Golgi initiates dephosphorylation  
255 of PI4P, which subsequently reduces the import of cholesterol sphingolipid into the Golgi<sup>20,39</sup>.

256 To visualize turnover of these signaling molecules, we transfected RAW 264.7 wildtype  
257 and Sptlc2 knockout cells with biosensors that specifically bind PIP2 and PIP3, and used live  
258 imaging to examine their dynamics during phagocytosis of Alexa55 labeled Zymosan A particles.  
259 The first such biosensor we used consisted of the fusion of GFP to the plekstrin homology (PH)  
260 domain of phospholipase C-delta (PLC $\delta$ ), which selectively binds to PIP2 (PH(PLC $\delta$ )-GFP)<sup>7</sup>. We  
261 show an enrichment of GFP signal to the site of particle engagement as wildtype cells synthesize  
262 PIP2 following particle recognition, and that this synthesis peaks with the engulfment of the  
263 particle (Figure 5D and E and Supplemental Movie 3). In Sptlc2<sup>-/-</sup> cells, however, we observe only  
264 a transient (and futile) accumulation of GFP signal and fails to accumulate to the same degree as  
265 in wildtype cells – and thus appear fail to synthesize PIP2 (Figure 5D and E and Supplemental  
266 Movie 4).

267 We then transfected RAW 264.7 cells with a PIP3 biosensor consisting of the PH domain  
268 of Akt fused to GFP (PH(AKT)-GFP)<sup>40</sup>. We visualized the localization of biosensor signal to show  
269 that wildtype cells begin synthesizing PIP3 early in phagocytosis, and that this synthesis strongly  
270 peaks as a particle is fully engulfed (Figure 5F and G and Supplementary Movie 5). However,  
271 Sptlc2 knockout cells fail to produce a trailing wave of PIP3, and thus never reach the levels of  
272 synthesis observed in wildtype cells (Figure 5F and G and Supplementary Movie 6).

273 Together, these results support the hypothesis that active sphingolipid biosynthesis is  
274 required for the initiation of the phagocytic signaling cascade, as well as for the transduction of  
275 pro-phagocytic signaling.

276

277 **Sphingomyelin biosynthesis is required for efficient Mtb uptake**

278        Which sphingolipid is most essential for enabling phagocytic signaling? Because  
279        sphingomyelin is highly enriched to the exoplasmic leaflet of the plasma membranes, we  
280        hypothesized that this lipid species is responsible for reduced Mtb uptake in cells depleted of total  
281        sphingolipids<sup>11,24,41</sup>. Sphingomyelin constitutes a major branch of the sphingolipid biosynthetic  
282        pathway, and the majority of its synthesis is catalyzed by the enzyme sphingomyelin synthase 1  
283        (SGMS1) in the Golgi – as such, cells may be depleted of this specific lipid species through  
284        CRISPR/Cas9-mediated knockout of this gene. Two SGMS1 CRISPR/Cas9 knockout clones of  
285        U937 cells that were isolated as previously described<sup>42</sup>. Using these SGMS1 knockouts, we  
286        performed Mtb uptake assays as described above. We found that SGMS1<sup>-/-</sup> cells are reduced in  
287        their capacity to uptake Mtb to a similar degree as to that of cells deficient in the biosynthesis of  
288        all sphingolipids (Figure 6A and B, and Figure 2A and B).

289        To address the possibility that other sphingolipids beyond sphingomyelin play roles in the  
290        phagocytosis of Mtb, we used CRISPR-Cas9 to knock out UDP-glucose ceramide  
291        glycosyltransferase (UGCG) in THP-1 cells (Figure 6C and D). UGCG is singularly responsible  
292        for catalyzing the synthesis of glucosylceramide – which is in turn the precursor of complex  
293        glycosphingolipids, a branch of sphingolipid biosynthesis comprising over 400 known lipid  
294        species<sup>43</sup>. If any of these species play a significant role in the phagocytic uptake of Mtb, we  
295        hypothesized that the inhibition of glycosphingolipid synthesis would result in a decrease in Mtb  
296        internalization. We found that two UGCG<sup>-/-</sup> clones displayed no change in the rate of Mtb  
297        phagocytosis, as compared to wildtype THP-1 cells (Figure 6C and D). Together, these data  
298        suggest that sphingomyelin is particularly essential for the phagocytic uptake of Mtb.

299

300 **Discussion**

301 In this study, we report that the capacity of Mtb to invade host cells by engagement of  
302 phagocytic receptors is significantly dependent on active sphingolipid biosynthesis pathway. Our  
303 central findings are thus: First, the blockade of total sphingolipid synthesis reduces Mtb uptake by  
304 approximately 50%. Critically, we show that blocking sphingolipid biosynthesis has no effect on  
305 the macropinocytosis of Herpes Simplex Virus – suggesting that these cells remain otherwise  
306 susceptible to infection via other routes of cellular uptake. We next show that blocking  
307 sphingolipid synthesis results in defects in the exclusion of the regulatory phosphatase CD45 at  
308 the phagocytic synapse. Furthermore, we show that several critical stages of phagocytic signaling  
309 involving GTPase activation and phosphoinositide turnover are perturbed upon depletion of  
310 sphingolipid synthesis, resulting in defective phagosome formation. And finally, we show that the  
311 blockade of sphingomyelin synthesis produces a phenocopy of total sphingolipid depletion –  
312 suggesting that sphingomyelin specifically is an essential lipid factor during Mtb uptake.

313 These data support a model in which sphingolipids are essential for successful activation  
314 of signaling events upon binding of pathogen-particles such as Mtb – and are thereby critical in  
315 initiating phagocytic synapse. Sphingolipids are instrumental in the accumulation of activated  
316 pathogen recognition receptor at the site of particle binding. This receptor accumulation is in turn  
317 essential for activating the phagocytic signaling cascade – including the activation of Rho GTPases  
318 and the turnover of phosphoinositides. Without active sphingolipid biosynthesis, there is an overall  
319 defect in phagosome formation and a reduction in phagocytic uptake of Mtb – though we find it  
320 notable that the lack of sphingolipid biosynthesis does not completely ablate the invasive  
321 phagocytosis of Mtb. We postulate that this may be partially due to the activity of the sphingolipid  
322 salvage pathways, which allow cells to acquire high-order sphingolipids from the surrounding

323 environment (e.g. fetal calf serum in growth media) and incorporate these species into the cellular  
324 lipid pool. Ongoing work seeks to address this hypothesis.

325 This study represents the first evidence for sphingolipids as regulators of signaling during  
326 phagocytosis of particles such as Zymosan and Mtb. We have previously reported that active  
327 sphingolipid biosynthesis is critical for the phagocytic clearance of *Candida albicans* both *in vitro*  
328 and *in vivo* – though we found no insight into the mechanism behind this defect in uptake. Further,  
329 a recent report suggests that treatment with FB1 results in reduced entry of *M. smegmatis* by  
330 J774A.1 cells (whereas there was no effect on the entry of *E. coli*)<sup>44</sup>. Adding an additional layer of  
331 complexity, another study suggests that blocking sphingolipid synthesis via treatment with FB1  
332 results in enhanced phagocytosis of opsonized particles<sup>22</sup>. We postulate that these data suggest a  
333 paradigm in which sphingolipids serve differing roles during the phagocytic uptake of different  
334 particles: enhancing the internalization of some, and limiting that of others.

335 Together, we show the dependency of Mtb on the sphingolipid biosynthetic pathway to  
336 efficiently enter and invade the host cells. In this context, phagocytosis represents a double-edged  
337 sword: while this immune process is critical for the clearance of many pathogenic particles, Mtb  
338 harnesses phagocytosis to gain entry to host cells and establish long-term survival. This study  
339 represents an important step towards understanding the underlying mechanisms of cellular  
340 processes mediating the earliest stage of Mtb invasion and contributes to the development of new  
341 strategies to fight this ancient pathogen.

342

343 **Acknowledgements**

344 This work is supported through the National Institutes of Health (3R21AI124225-01A1)  
345 and the Medical Research Foundation. We would like to thank the labs of Dr. David Underhill  
346 (Cedars-Sinai Medical Center, Los Angeles, CA), Dr. Sergio Grinstein (The Hospital for Sick  
347 Children Research Institute, Toronto, ON), Dr. Sebastian Winter (Max Planck Institute of  
348 Biochemistry, Munich, Germany), Dr. Tim Nice (Oregon Health and Science University,  
349 Portland, OR), and Dr. David Johnson (Oregon Health and Science University, Portland, OR) for  
350 kindly providing reagents, cell lines, viruses, and plasmid constructs essential to the completion  
351 of this study. We would also like to thank the members of the OHSU Cores for Advanced Light  
352 Microscopy and Flow Cytometry for assistance and training in data collection and analysis – in  
353 particular, we would like to thank Dr. Stefanie Kaech Petrie, Matthew Lewis, and Sara  
354 Christensen. We would finally like to thank Madeleine Faucher, Marie Foss, and Jossef Osborn  
355 who kindly and patiently assisted in the editing and preparation of this work.

356

357 **Conflicts of interest**

358 The authors have no conflicts of interest to declare.

359

360

361

362

363

364 **Materials and Methods**

365 **Reagents.**

366 Myriocin and FB1 were purchased from Cayman Chemical Company. 3-L-[<sup>14</sup>C]-serine  
367 was purchased from American Radioactivity. Phorbol 12-myristate 13-acetate (PMA) was  
368 purchased from BioLegend. 4% paraformaldehyde was from Fisher Scientific. DyLight® 488  
369 Phalloidin was purchased from Cell Signaling Technology, and Alexa Fluor 647-conjugated  
370 Zymosan A (*S. cerevisiae*) BioParticles were purchased from Thermo Fisher. Mouse Monoclonal  
371 antibody against GAPDH (ab8245) was purchased from Abcam. Anti-rabbit IgG HRP-linked  
372 antibody and anti-mouse IgG HRP-linked antibody were purchased from Cell Signaling. APC-  
373 conjugated, rat monoclonal antibody against CD45 antibody (Clone 30-F11) was purchased from  
374 Biolegend. FITC-conjugated, rat monoclonal antibody against Dectin-1 (Clone 2A11) was  
375 purchased from AbD Serotec. Zombie Aqua™ Fixable Viability Kit (part #77143) was purchased  
376 from BioLegend.

377

378 **Plasmids**

379 The plasmids used for generation of lentivirus consists of the pCDH-CMV(-)-sgRNA plasmid, the  
380 psPAX2 (packaging) and pMD2.G (envelope) plasmids. pCW-Cas9 lentivirus was purchased from  
381 Addgene. The pMXsIP-Dectin-1-GFP was kindly provided by the lab of Dr. David Underhill  
382 (Cedars-Sinai Medical Center, Los Angeles, CA)<sup>45</sup>. Active (GTP-bound) Rac1/Cdc42 was  
383 detected with PAK(PBD)-YFP, a plasmid encoding the PBD of PAK fused to YFP<sup>37</sup> was obtained  
384 from Addgene. PI(4,5)P2 was detected with PH(PLC $\delta$ )-GFP, a plasmid encoding the PH domain  
385 of PLC $\delta$  fused to GFP. PI(3,4,5)P3 levels were monitored by PH(AKT)-GFP, a plasmid encoding

386 the PH domain of AKT fused to GFP<sup>46</sup>. These two fusion constructs were kindly provided by the  
387 lab of Dr. Sergio Grinstein (The Hospital for Sick Children Research Institute, Toronto, ON).

388

### 389 **Cell culture and small molecule inhibitor treatment**

390 THP-1, U937, and DC2.4 cells were routinely cultured in RPMI medium supplemented  
391 with 10% FBS (Seradigm) and 1% Pen Strep (Gibco). RAW 264.7 cells were cultured in DMEM  
392 supplemented with 10% FBS and 1% PenStrep. All cell lines were cultured at 37 °C and 5% CO<sub>2</sub>.  
393 In plating adherent cells (RAW 264.7 and DC2.4), cells were lifted using 0.25% trypsin solution  
394 (Gibco) and counted using hemocytometer, with Trypan Blue solution (Gibco) for counterstain.

395 THP-1 and U937 cells were differentiated to macrophages by 50ng/ml PMA for 1 day in  
396 RPMI medium supplemented with 10% FBS, after which the cells were treated with 5μM myriocin  
397 or FB1 for 3 days in RPMI supplemented with 10% FBS and 1%Pen Strep. RAW 264.7 and DC2.4  
398 cells were treated similarly with myriocin and FB1 – however, 24-hours before infection, cells  
399 were lifted and counted, and seeded at appropriate density in 96-well plates or on coverslips.  
400 Biological replicates represent independent treatments with chemical inhibitors and infections on  
401 separate days.

402

### 403 **Metabolic labeling and thin layer chromatography**

404 5x10<sup>5</sup> cells (wildtype, knockout, or inhibitor-treated) were seeded into a 6-well plate. Cells  
405 were labeled with 1μCi/ml of 3-L-[<sup>14</sup>C]-serine for 4 hours in Opti-MEM supplemented with the  
406 appropriate inhibitors. Cells were then washed two times with PBS and lipid extraction was done  
407 following the Bligh and Dyer method<sup>47</sup>. The methanol/chloroform-lipid extracts were dried by  
408 nitrogen gas. Dried lipids were re-dissolved in several drops of chloroform/methanol (1:2, vol/vol)

409 and loaded on a TLC plate. Lipids were separated by developing the TLC plate first in acetone and  
410 then in a mixture of chloroform, methanol and 25% ammonia solution (50:25:6, vol/vol/vol).  
411 Radiolabeled lipids were detected on a Storm 825 Phosphor-Imager (GE Healthcare).

412

#### 413 **Generation of lentiviruses**

414 Lentivirus production was performed as described previously<sup>48</sup>. Briefly, lentiviruses were  
415 produced by co-transfection of HEK 293T cells with the lentiviral vectors that contain our gene of  
416 interest (pCDH-sgRNA or pCW-Cas9) and the packaging plasmids (psPAX2 and pMD2.G).  
417 Transfection was performed with Lipofectamine 3000 (Thermo Fisher) according to  
418 manufacturer's instructions. Cells were cultured in DMEM supplemented with 10%FBS and the  
419 growth medium was replaced after 6 hours. 48 hours after transfection, lentivirus-containing  
420 supernatants were harvested, centrifuge for 5min at 1250 rpm and filtered through a 0.45μm filter.

421

#### 422 **Generation of CRISPR/Cas9-mediated knockout cell lines**

423 CRISPR/Cas9-mediated genome-editing for genes involved in the sphingolipid pathway  
424 were performed as described previously<sup>8</sup>. Briefly, to generate Sptlc2<sup>-/-</sup> knockout RAW 264.7 cells  
425 were infected with lentivirus (pCW-Cas9) encoding Cas9 cDNA, and were cultured in media  
426 containing 2 μg/mL of puromycin (Sigma Aldrich). Potential target sequences for CRISPR  
427 interference were found with the rules outlined in Mali et al. 2013<sup>49</sup>. The following seed sequences  
428 (CRISPR target sequences) preceding the PAM motif that were found in the exon of Sptlc2 gene  
429 were used: Sptlc2 #1 GAACGGCTGCGTCAAGAAC; Sptlc2 #2:  
430 AGCAGCACCGCCACCGTCG; UGCG GCTGTGGCTGATGCATTCA. Potential off-target  
431 effects of the seed sequence were evaluated using the NCBI Mus musculus Nucleotide BLAST.

432 Generation of CRISPR/Cas9-mediated Sptlc2-knockout RAW 264.7 cell line and UGCG-  
433 knockout THP-1 cell line were performed as previously described<sup>48</sup>. Briefly, CRISPR gBlock was  
434 designed to clone into the restriction enzymatic site NheI/BamHI of pCDH-CMV(-) (SBI;  
435 CD515B-1) as follows:

436 cacagtccagacagtgactcaGTGTCACAGctagcTTTCCCATGATTCTTCATATTGCATAT  
437 ACGATACAAGGCTGTTAGAGAGATAATTAGAATTAATTGACTGTAAACACAAAGA  
438 TATTAGTACAAAATACGTGACGTAGAAAGTAATAATTCTGGGTAGTTGCAGTT  
439 TAAAATTATGTTTAAAATGGACTATCATATGCTTACCGTAAC TGAAAGTATTG  
440 ATTTCTGGCTTATATCTTGAAAGGACGAAACACCGnnnnnnnnnnnnnnnnnG  
441 TTTAGAGCTAGAAATAGCAAGTTAAAATAAGGCTAGTCCGTTATCAACTGAAAAA  
442 GTGGCACCGAGTCGGTGCTTTTTggatccTGTGCACAGtcagtcacagtctac (n: CRISPR  
443 target sequences).

444 The gBlock was then digested using the restriction enzymes NheI and BamHI and ligated  
445 into pCDH-CMV(-) vector that was linearized by digesting with the same restriction enzyme.

446 The Cas9-inducible cells were infected with lentivirus carrying pCDH-CMV(-)-sgRNA,  
447 and were cultured in media containing 250 µg/mL of hygromycin B (Life Technology). To induce  
448 expression of Cas9, cells were treated with 1 µg/mL of doxycycline (Clontech) for 3–5 days.  
449 Clonal selection was performed by single cell dilution on 96-well plates. The individual colonies  
450 were collected and the expression of Sptlc2 was examined by western-blotting using Sptlc2  
451 antibody.

452 U937 SGSM1<sup>-/-</sup> cells were kindly provided by Sebastian Virreira Winter (Max Planck  
453 Institute of Biochemistry, Munich, Germany) and the CRISPR/Cas9-mediated knock out cell lines  
454 were established as described in Winter et al., 2016<sup>42</sup>.

455

456 **Culturing of Mtb**

457        Culturing and infection of Mtb was conducted in a Biosafety-level 3 laboratory following  
458 general safety guidelines. Mtb strain H37R, expressing constitutively mCherry were obtained from  
459 the Fortune lab (Ragon Institute, Cambridge, MA). It was cultured at 37°C in 7H9 Broth medium  
460 supplemented with 50µg/ml hygromycin B. The density of the bacteria at the time of infection is  
461 between OD600 of 0.6 - 0.8.

462

463 **Mtb uptake assay**

464        For infection of THP-1 and U937 cells, the cells were seeded into a SensoPlate™ 96-Well  
465 Glass-Bottom Plates (Greiner Bio-One) at a density of  $1.5 \times 10^4$  cells per well in RPMI  
466 supplemented with 10% FBS, 1% PenStrep and 50ng/ml PMA at 37°C. One day after  
467 differentiation, cells were treated for 3 days with 5µM myriocin or 15µM FB1. These cells were  
468 then infected with a multiplicity of infection (MOI) of 10 in RPMI supplemented with 10% FBS  
469 for 2 hours at 37°C.

470        For infection of RAW 264.7 and DC2.4 cells,  $2.0 \times 10^4$  cells per well were seeded into a  
471 SensoPlate™ 96-Well Glass-Bottom Plates (Greiner Bio-One). 24 hour later, the cells were were  
472 infected with an MOI of 10 in RPMI supplemented with 10% FBS for 2 hours at 37°C. Cells were  
473 washed with PBS, and then fixed with 4% PFA over night at 4°C.

474

475 **Phagocytosis measurement assay**

476        Phagocytosis assay was performed as previously described<sup>50</sup>. Briefly, fixed cells were  
477 washed twice with PBS and incubated in PBS for 15 min in Permeabilization Buffer (0.1% Triton

478 X-100 and 1%BSA). Cells were stained with Phalloidin-Alexa 488 (Thermo Fisher) at a final  
479 concentration of 33nM for 60 min and washed one time with PBS. After the Phalloidin-staining,  
480 cells were stained with DAPI for 10 mins and washed 3 times with PBS. Cells were then imaged  
481 using the Keyence BZ-X700 with a PlanFluor 20x objective. The parameters for imaging were  
482 kept the same for each sample. For image analysis the Keyence BZ-X Analyzer software was used.  
483 In brief: The outline of the cells was determined via the Alexa488 signal (Phalloidin staining) and  
484 the number and area of mCherry (Mtb) signal in the Alexa488 signal was detected by the program.  
485 In a second round the number of cells was determined by counting the nuclei via the DAPI staining.  
486 Number of bacteria (mCherry-signal) inside the cell was divided by the number of cells (DAPI  
487 signal) to identify the phagocytosis efficiency.

488

#### 489 **Live imaging of phagocytosis**

490 For transient transfection, RAW 264.7 cells were seeded into a SensoPlate™ 96-Well  
491 glass-bottom plates at a cell number of  $1.0 \times 10^4$  cells/well 24 hours prior transfection. Transfection  
492 was conducted with Lipofectamine 3000 according to manufacturer's instructions. For imaging,  
493 the growth medium was aspirated and replaced with RPMI without phenol red containing Zymosan  
494 A Bioparticles Alexa595 at an MOI of 10. The 96-well plates were centrifuged at 1000rpm for one  
495 minute. The cells were imaged with the SDC microscope (Nikon) and 3-4 different spots per well  
496 were imaged at the same time for 60 min with capture intervals of 15 sec. The parameters for  
497 imaging were kept the same for each sample.

498

#### 499 **Live image analysis (quantification)**

500 Of live cell images, individual images were selected for further analysis if they captured a  
501 cell bound to a Zymosan particle while maintaining a healthy morphology throughout the imaging  
502 time-course. Imaging analysis was performed using FIJI software<sup>51</sup>. The parameters for image  
503 processing were kept constant when comparing different data sets. The area of the phagosome was  
504 selected, cropped and opened in a new window. The threshold at different time points was  
505 measured by the analyze-measure function of FIJI. The values for the GFP-threshold of the  
506 phagosome area were divided by the values for the GFP-threshold of the whole cell at the  
507 corresponding time points.

508

#### 509 **Dectin-1 and CD45 displacement assay**

510 RAW 264.7 WT and Sptlc2<sup>-/-</sup> cells were seeded on glass coverslips in 12-well plates and  
511 grown to 70-90% confluence overnight. Cells were transfected with pMXsIP Dectin-1-GFP  
512 using Lipofectamine 3000 (Invitrogen) according to the manufacturer's instructions. After 24  
513 hrs, cells were washed three times with ice-cold PBS, kept on ice for 5 min, and inoculated with  
514 Alexa Fluor 594-conjugated Zymosan in chilled serum-free DMEM at a ratio of 10 beads per  
515 cell. After centrifugation for 5 min at 250 x g and 4°C, cells were incubated for 5 min at 37°C,  
516 washed three times with ice-cold PBS to remove unbound Zymosan, then fixed for 15 min with  
517 4% paraformaldehyde.

518 Images were collected using an LSM880 confocal microscope using a PLAN APO 63x oil-  
519 immersion objective and AIRY SCAN. Image analysis was performed using FIJI. Briefly, a  
520 region-of-interest was defined around the Zymosan particle, and Pearson's correlation coefficient  
521 between Dectin-1-GFP signal and anti-CD45-APC signal was calculated using the colocalization  
522 function.

523

524 **Flow cytometry**

525 RAW 264.7 wildtype and Sptlc2<sup>-/-</sup> cells were rinsed with PBS and lifted from the flask  
526 using treatment with trypsin. Fc receptor was blocked with CD16/32 antibody (1:100) and cells  
527 were stained with ZombieAqua Live/Dead (1:200). Cells were then stained with either CD45-  
528 APC (1:200), or Dectin-1-FITC (1:50) for 30 min. Finally, cells were fixed for 20 mins in 4%  
529 paraformaldehyde and analyzed using an LSR-II flow cytometer. Cells independently stained  
530 with ZombieAqua, CD45-APC, and Dectin-1-FITC were used for compensation. Analysis was  
531 performed using FlowJo software.

532

533 **Herpes Simplex Virus-1 infection**

534 HSV-1-mCherry reporter virus was kindly provided by the lab of Dr. David Johnson  
535 (Oregon Health and Science University, Portland, Oregon). Twenty-four hours prior to infection,  
536 1x10<sup>4</sup> wildtype and Sptlc2 knockout RAW 264.7 cells were seeded on glass coverslips in a 12-  
537 well plate. Cells were equally infected at an MOI ~1, and incubated for 12 hours at 37°C and 5%  
538 CO<sub>2</sub>. Coverslips were fixed for 20 mins in 4% paraformaldehyde, stained with DAPI and then  
539 imaged on a Keyence BZ-X700. Infection rates were calculated by dividing the mCherry  
540 expressing cells with the total number of cells (DAPI signal).

541

542

543

544            **References**

545

- 546    1. Daniel, T. M. The history of tuberculosis. *Respir. Med.* **100**, 1862–1870 (2006).
- 547    2. *Global tuberculosis report 2018.* (2018).
- 548    3. Korb, V., Chuturgoon, A. & Moodley, D. Mycobacterium tuberculosis: Manipulator of  
549        Protective Immunity. *Int. J. Mol. Sci.* **17**, 131 (2016).
- 550    4. Ouimet, M. *et al.* Mycobacterium tuberculosis induces the miR-33 locus to reprogram  
551        autophagy and host lipid metabolism. *Nat. Immunol.* **17**, 677–686 (2016).
- 552    5. Fine-Coulson, K., Reaves, B. J., Karls, R. K. & Quinn, F. D. The Role of Lipid Raft  
553        Aggregation in the Infection of Type II Pneumocytes by Mycobacterium tuberculosis.  
554        *PLoS One* **7**, (2012).
- 555    6. Thompson, C. R. *et al.* Sphingosine Kinase 1 (SK1) Is Recruited to Nascent Phagosomes  
556        in Human Macrophages: Inhibition of SK1 Translocation by Mycobacterium tuberculosis.  
557        *J. Immunol.* **174**, 3551–3561 (2005).
- 558    7. Levin, R., Grinstein, S. & Schlam, D. Phosphoinositides in phagocytosis and  
559        macropinocytosis. *Biochim. Biophys. Acta - Mol. Cell Biol. Lipids* **1851**, 805–823 (2015).
- 560    8. Tafesse, F. G. *et al.* Disruption of Sphingolipid Biosynthesis Blocks Phagocytosis of  
561        Candida albicans. *PLoS Pathog.* **11**, 1–27 (2015).
- 562    9. Malik, Z. A. *et al.* Cutting Edge: Mycobacterium tuberculosis Blocks Ca<sup>2+</sup> Signaling and  
563        Phagosome Maturation in Human Macrophages Via Specific Inhibition of Sphingosine  
564        Kinase. *J. Immunol.* **170**, 2811–2815 (2003).
- 565    10. Gatfield, J. & Pieters, J. Essential role for cholesterol in entry of mycobacteria into  
566        macrophages. *Science* **288**, 1647–50 (2000).

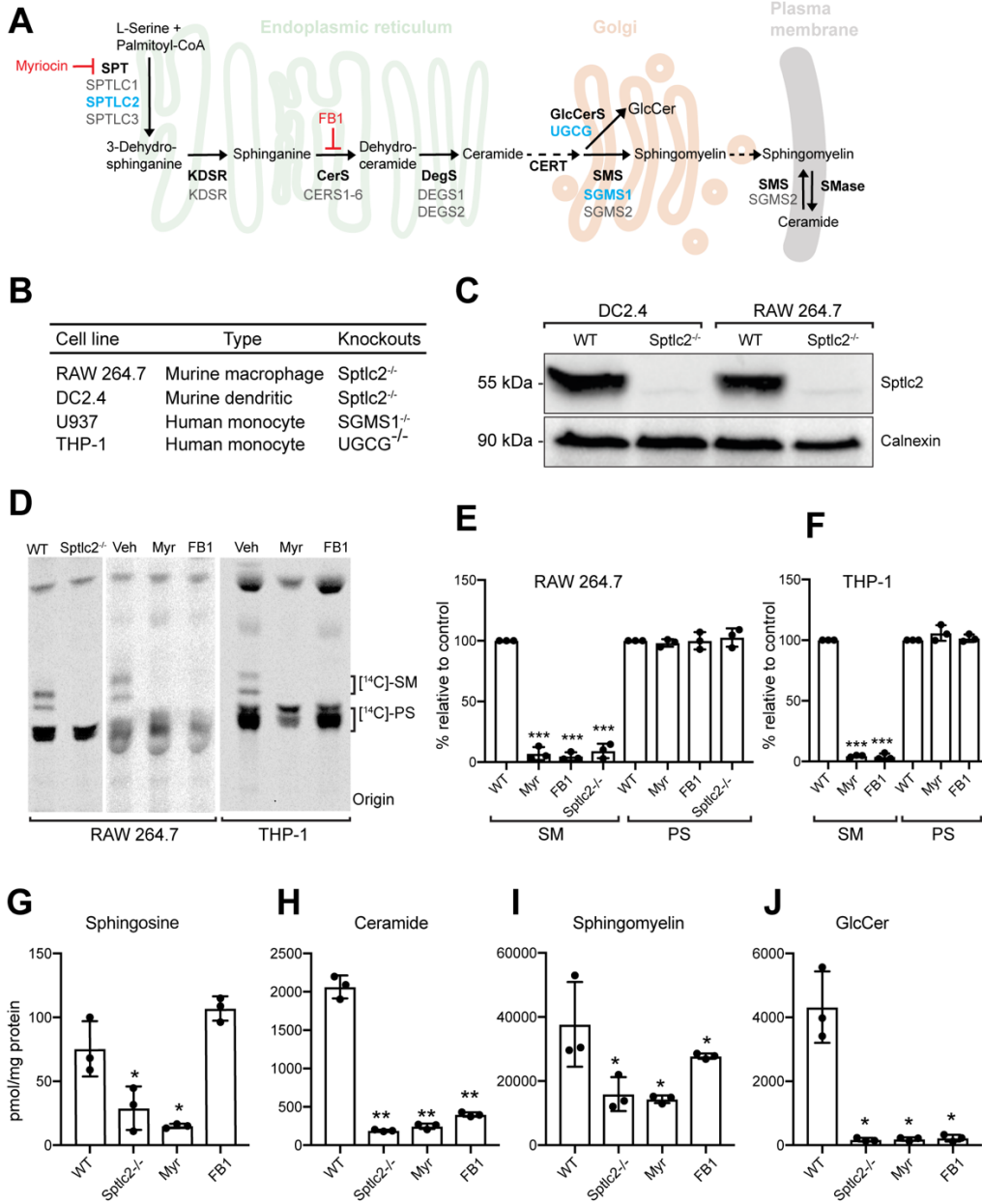
- 567 11. Kinoshita, M., Suzuki, K. G. N., Murata, M. & Matsumori, N. Evidence of lipid rafts  
568 based on the partition and dynamic behavior of sphingomyelins. *Chem. Phys. Lipids* **215**,  
569 84–95 (2018).
- 570 12. García-Arribas, A. B., Alonso, A. & Goñi, F. M. Cholesterol interactions with ceramide  
571 and sphingomyelin. *Chem. Phys. Lipids* **199**, 26–34 (2016).
- 572 13. El Alwani, M., Wu, B. X., Obeid, L. M. & Hannun, Y. A. Bioactive sphingolipids in the  
573 modulation of the inflammatory response. *Pharmacol. Ther.* **112**, 171–183 (2006).
- 574 14. Hla, T. & Dannenberg, A. J. Sphingolipid Signaling in Metabolic Disorders. *Cell Metab.*  
575 **16**, 420–434 (2012).
- 576 15. Taha, T. A., Mullen, T. D. & Obeid, L. M. A house divided: Ceramide, sphingosine, and  
577 sphingosine-1-phosphate in programmed cell death. *Biochim. Biophys. Acta - Biomembr.*  
578 **1758**, 2027–2036 (2006).
- 579 16. Hakomori, S. I. & Igarashi, Y. Functional role of glycosphingolipids in cell recognition  
580 and signaling. *J. Biochem.* **118**, 1091–1103 (1995).
- 581 17. Hannun, Y. A. & Obeid, L. M. The ceramide-centric universe of lipid-mediated cell  
582 regulation: Stress encounters of the lipid kind. *J. Biol. Chem.* **277**, 25847–25850 (2002).
- 583 18. Snider, A. J., Alexa Orr Gandy, K. & Obeid, L. M. Sphingosine kinase: Role in regulation  
584 of bioactive sphingolipid mediators in inflammation. *Biochimie* **92**, 707–715 (2010).
- 585 19. Leier, H. C., Messer, W. B. & Tafesse, F. G. Lipids and pathogenic flaviviruses : An  
586 intimate union. 1–7 (2018). doi:<https://doi.org/10.1371/journal.ppat.1006952>
- 587 20. Capasso, S. *et al.* Sphingolipid metabolic flow controls phosphoinositide turnover at the  
588 trans -Golgi network. *EMBO J.* **36**, 1736–1754 (2017).
- 589 21. Hinkovska-Galcheva, V., Boxer, L., Mansfield, P. J., Schreiber, A. D. & Shayman, J. A.

- 590                  Enhanced phagocytosis through inhibition of de novo ceramide synthesis. *J. Biol. Chem.*  
591                  **278**, 974–982 (2003).
- 592        22. Hinkovska-Galcheva, V., Boxer, L., Mansfield, P. J., Schreiber, A. D. & Shayman, J. A.  
593                  Enhanced Phagocytosis through Inhibition of de Novo Ceramide Synthesis. *J. Biol. Chem.*  
594                  **278**, 974–982 (2003).
- 595        23. Hanada, K. Serine palmitoyltransferase, a key enzyme of sphingolipid metabolism.  
596                  *Biochim. Biophys. Acta* **1632**, 16–30 (2003).
- 597        24. Gault, C., Obeid, L. & Hannun, Y. An overview of sphingolipid metabolism: from  
598                  synthesis to breakdown Introduction to Sphingolipid Metabolism. *Adv Exp Med Biol* **688**,  
599                  1–23 (2010).
- 600        25. Meivar-Levy, I., Sabanay, H., Bershadsky, A. D. & Futterman, A. H. The Role of  
601                  Sphingolipids in the Maintenance of Fibroblast Morphology. *J. Biol. Chem.* **272**, 1558–  
602                  1564 (2002).
- 603        26. Underhill, D. M. Macrophage recognition of zymosan particles. *J. Endotoxin Res.* **9**, 176–  
604                  180 (2003).
- 605        27. Mansour, M. K. *et al.* Dectin-1 Activation Controls Maturation of  $\beta$ -1,3-Glucan-  
606                  containing Phagosomes. *J. Biol. Chem.* **288**, 16043–16054 (2013).
- 607        28. Rothfuchs, A. G. *et al.* Dectin-1 Interaction with Mycobacterium tuberculosis Leads to  
608                  Enhanced IL-12p40 Production by Splenic Dendritic Cells. *J. Immunol.* **179**, 3463–3471  
609                  (2007).
- 610        29. Wagener, M., Hoving, J. C., Ndlovu, H. & Marakalala, M. J. Dectin-1-Syk-CARD9  
611                  Signaling Pathway in TB Immunity. *Front. Immunol.* **9**, (2018).
- 612        30. Wisner, T. W., Sugimoto, K., Howard, P. W., Kawaguchi, Y. & Johnson, D. C.

- 613        Anterograde Transport of Herpes Simplex Virus Capsids in Neurons by both Separate and  
614        Married Mechanisms. *J. Virol.* **85**, 5919–5928 (2011).
- 615        31. Tiwari, V. & Shukla, D. Nonprofessional Phagocytosis Can Facilitate Herpesvirus Entry  
616        into Ocular Cells. *Clin. Dev. Immunol.* **2012**, 1–8 (2012).
- 617        32. Clement, C. *et al.* A novel role for phagocytosis-like uptake in herpes simplex virus entry.  
618        *J. Cell Biol.* **174**, 1009–1021 (2006).
- 619        33. Gianni, T., Gatta, V. & Campadelli-Fiume, G. V 3-integrin routes herpes simplex virus to  
620        an entry pathway dependent on cholesterol-rich lipid rafts and dynamin2. *Proc. Natl.*  
621        *Acad. Sci.* **107**, 22260–22265 (2010).
- 622        34. Goodridge, H. S. *et al.* Activation of the innate immune receptor Dectin-1 upon formation  
623        of a ‘phagocytic synapse’. *Nature* **472**, 471–475 (2011).
- 624        35. Grassmé, H. *et al.* Host defense against *Pseudomonas aeruginosa* requires ceramide-rich  
625        membrane rafts. *Nat. Med.* **9**, 322 (2003).
- 626        36. Mao, Y. & Finnemann, S. C. Regulation of phagocytosis by Rho GTPases. *Small*  
627        *GTPases* **6**, 89–99 (2015).
- 628        37. Hoppe, A. D. & Swanson, J. A. Cdc42, Rac1, and Rac2 Display Distinct Patterns of  
629        Activation during Phagocytosis. *Mol. Biol. Cell* **15**, 3509–3519 (2004).
- 630        38. Schlam, D. *et al.* Phosphoinositide 3-kinase enables phagocytosis of large particles by  
631        terminating actin assembly through Rac/Cdc42 GTPase-activating proteins. *Nat. Commun.*  
632        **6**, 8623 (2015).
- 633        39. Hanada, K. *et al.* Molecular machinery for non-vesicular trafficking of ceramide. *Nature*  
634        **426**, 803–809 (2003).
- 635        40. Marshall, J. G. *et al.* Restricted Accumulation of Phosphatidylinositol 3-Kinase Products

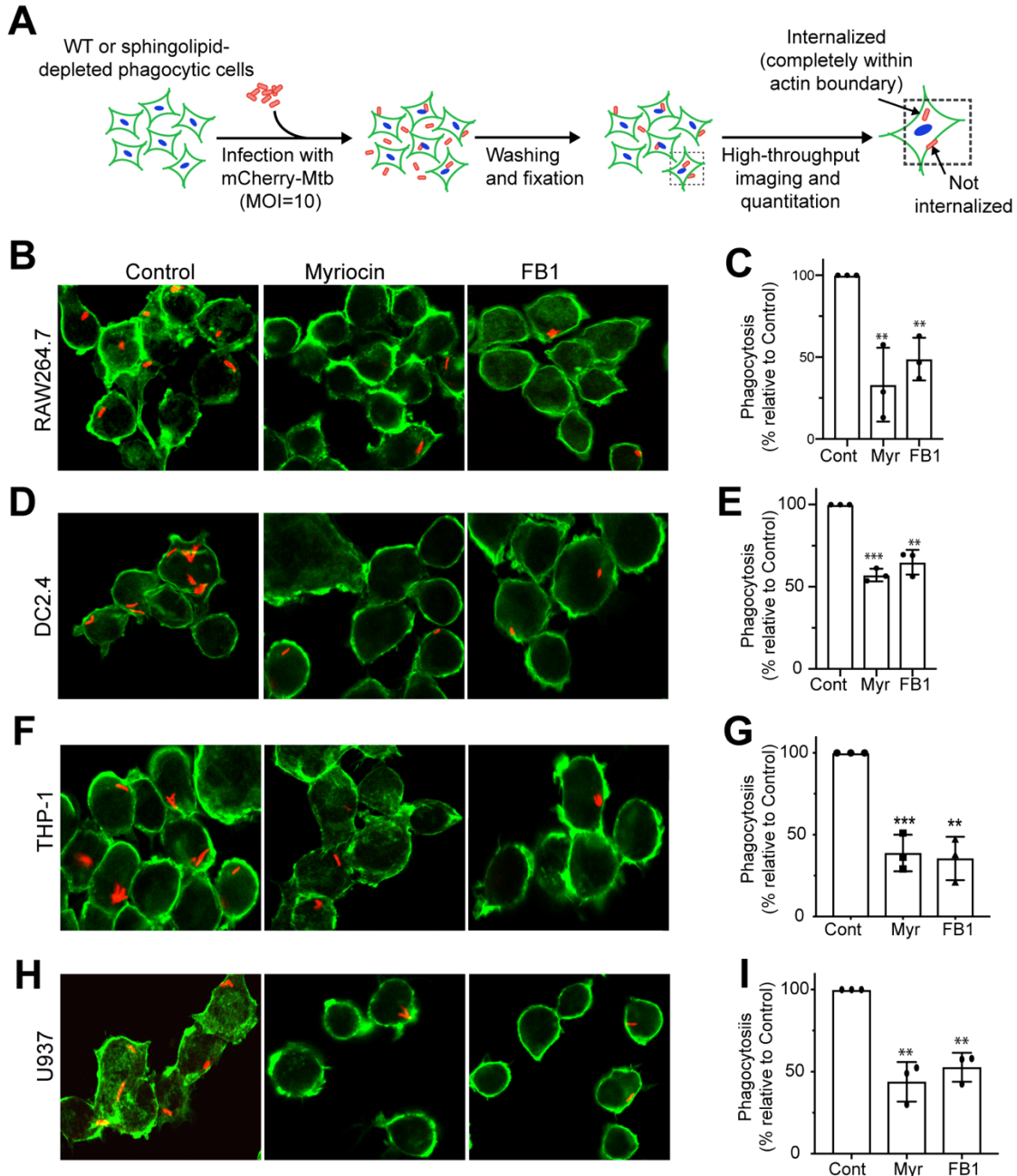
- 636           in a Plasmalemmal Subdomain during Fc $\gamma$  Receptor-Mediated Phagocytosis. *J. Cell Biol.*  
637           **153**, 1369–1380 (2001).
- 638     41. Subbaiah, P. V. & Sargis, R. M. Sphingomyelin: A natural modulator of membrane  
639           homeostasis and inflammation. *Med. Hypotheses* **57**, 135–138 (2001).
- 640     42. Virreira Winter, S., Zychlinsky, A. & Bardoel, B. W. Genome-wide CRISPR screen  
641           reveals novel host factors required for *Staphylococcus aureus*  $\alpha$ -hemolysin-mediated  
642           toxicity. *Sci. Rep.* **6**, 24242 (2016).
- 643     43. Wegner, M. S., Gruber, L., Mattjus, P., Geisslinger, G. & Grösch, S. The UDP-glucose  
644           ceramide glycosyltransferase (UGCG) and the link to multidrug resistance protein 1  
645           (MDR1). *BMC Cancer* **18**, 1–10 (2018).
- 646     44. Viswanathan, G., Jafurulla, M., Kumar, G. A., Raghunand, T. R. & Chattopadhyay, A.  
647           Macrophage sphingolipids are essential for the entry of mycobacteria. *Chem. Phys. Lipids*  
648           **213**, 25–31 (2018).
- 649     45. Goodridge, H. S. *et al.* Activation of the innate immune receptor Dectin-1 upon formation  
650           of a  $\tilde{\alpha}$ -Phagocytic synapse<sup>TM</sup>. *Nature* **472**, 471–475 (2011).
- 651     46. Feng, S. *et al.* A Rapidly Reversible Chemical Dimerizer System to Study Lipid Signaling  
652           in Living Cells. *Angew. Chemie Int. Ed.* **53**, 6720–6723 (2014).
- 653     47. BLIGH, E. G. & DYER, W. J. A rapid method of total lipid extraction and purification.  
654           *Can. J. Biochem. Physiol.* **37**, 911–7 (1959).
- 655     48. Tafesse, F. G. *et al.* GPR107, a G-protein-coupled Receptor Essential for Intoxication by  
656           Pseudomonas aeruginosa Exotoxin A, Localizes to the Golgi and Is Cleaved by Furin. *J.*  
657           *Biol. Chem.* **289**, 24005–24018 (2014).
- 658     49. Mali, P. *et al.* RNA-guided human genome engineering via Cas9. *Science* **339**, 823–6  
659           (2013).

- 660 50. Rashidfarrokhi, A., Richina, V. & Tafesse, F. G. Visualizing the Early Stages of  
661 Phagocytosis. *J. Vis. Exp.* (2017). doi:10.3791/54646
- 662 51. Schindelin, J. *et al.* Fiji: an open-source platform for biological-image analysis. *Nat.*  
663 *Methods* **9**, 676–682 (2012).
- 664
- 665



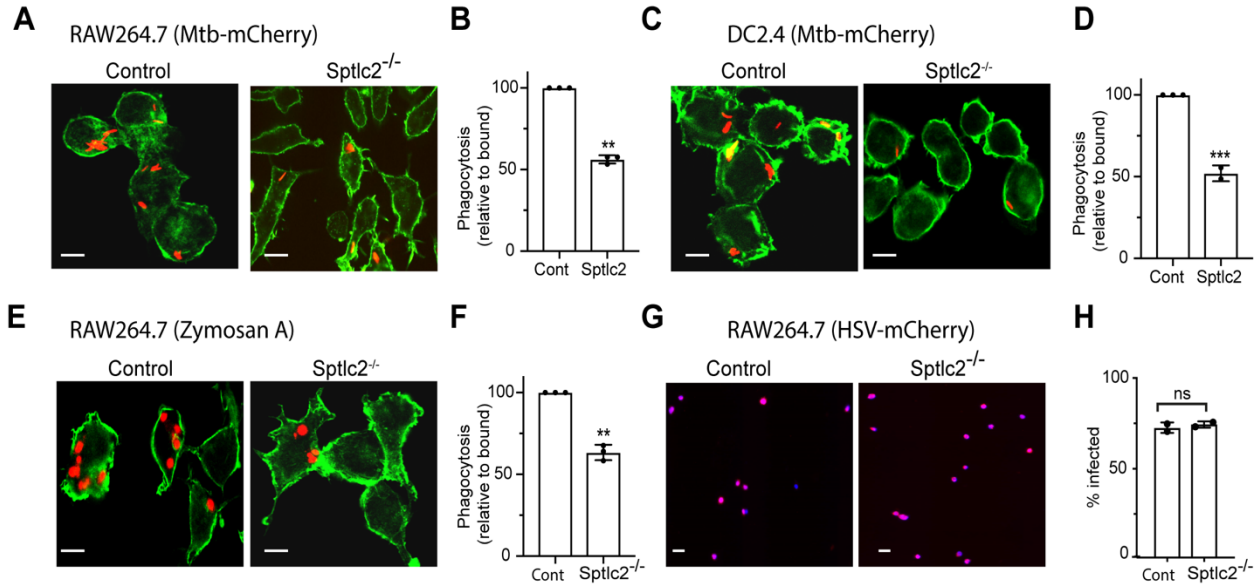
666

667 **Figure 1: Manipulation of cellular sphingolipid levels using genetics and chemical tools. (A)**  
 668 Simplified overview of sphingolipid biosynthetic pathway. Genes that are deleted using CRISPR/Cas9  
 669 system are indicated in blue and the inhibitors that are used in this study are shown in red. (B) Model  
 670 phagocytic cell lines used in this study, respective species background, and genetic knockouts available.  
 671 (C) Western blot probed using anti-Sptlc2 antibody in wildtype and CRISPR/Cas9 knockout DC2.4 and  
 672 RAW 264.7 cells (upper), and probed against calnexin as loading control (lower). (D) Control, mutant  
 673 and inhibitor-treated cells were labeled with the sphingolipid precursor 3-L-[<sup>14</sup>C]-serine, and total lipids  
 674 were extracted and analyzed by thin layer chromatography (TLC) and autoradiography. (E, F)  
 675 Quantification of the [<sup>14</sup>C]-SM and [<sup>14</sup>C]-PS signals from [<sup>14</sup>C]-serine labeling of RAW264.7 and THP-1  
 676 cells shown in D. (G-J) Total lipids were extracted from control, Sptlc2<sup>-/-</sup> and inhibitor-treated cells and  
 677 lipid profiling was performed using LC/MS. Levels of sphingosine (G), ceramide (H), sphingomyelin (I)  
 678 and glucosylceramide (GlcCer) are shown. All graphs display SD of three independent experiments, and  
 679 an unpaired t-test was used to analyze the significance of the data. \*p<0.05, \*\*p<0.01, \*\*\* p < 0.001.



680

681 **Figure 2: Sphingolipid biosynthesis is required for efficient phagocytosis of Mtb.** (A) Overview of  
 682 the phagocytosis experiment. (B, D) Representative images of Mtb-infected RAW 264.7 (B) and DC2.4  
 683 (D) cells. (C, E) Quantification of Mtb uptake in RAW 264.7 (C) and DC2.4 (E) cells. (F, H)  
 684 Representative images of infected THP-1 (F) and U937 (H) monocyte-derived macrophages. 2x10<sup>4</sup> THP-  
 685 1 and U937 cells were plated in 96-well plate and were differentiated using 80ng/ml PMA for one day,  
 686 and then treated for three days with myriocin or FB1. (G, I) Quantification of Mtb uptake in THP-1 (G)  
 687 and U937 (I) cells. Three independent experiments were performed each in triplicate with at least 1,000  
 688 cells quantified per replicate. Mtb uptake was defined using total number of bacteria (mCherry signal)  
 689 within cellular periphery (Phalloidin-Alexa488 signal) and cellular counts were defined by nuclear stain.  
 690 Data are mean ± SD. \*\*\*p<0.001, two-tailed unpaired t-test. Data are mean ± SD. \*\*p<0.01, \*\*\*p<0.001,  
 691 two-tailed unpaired t-test.

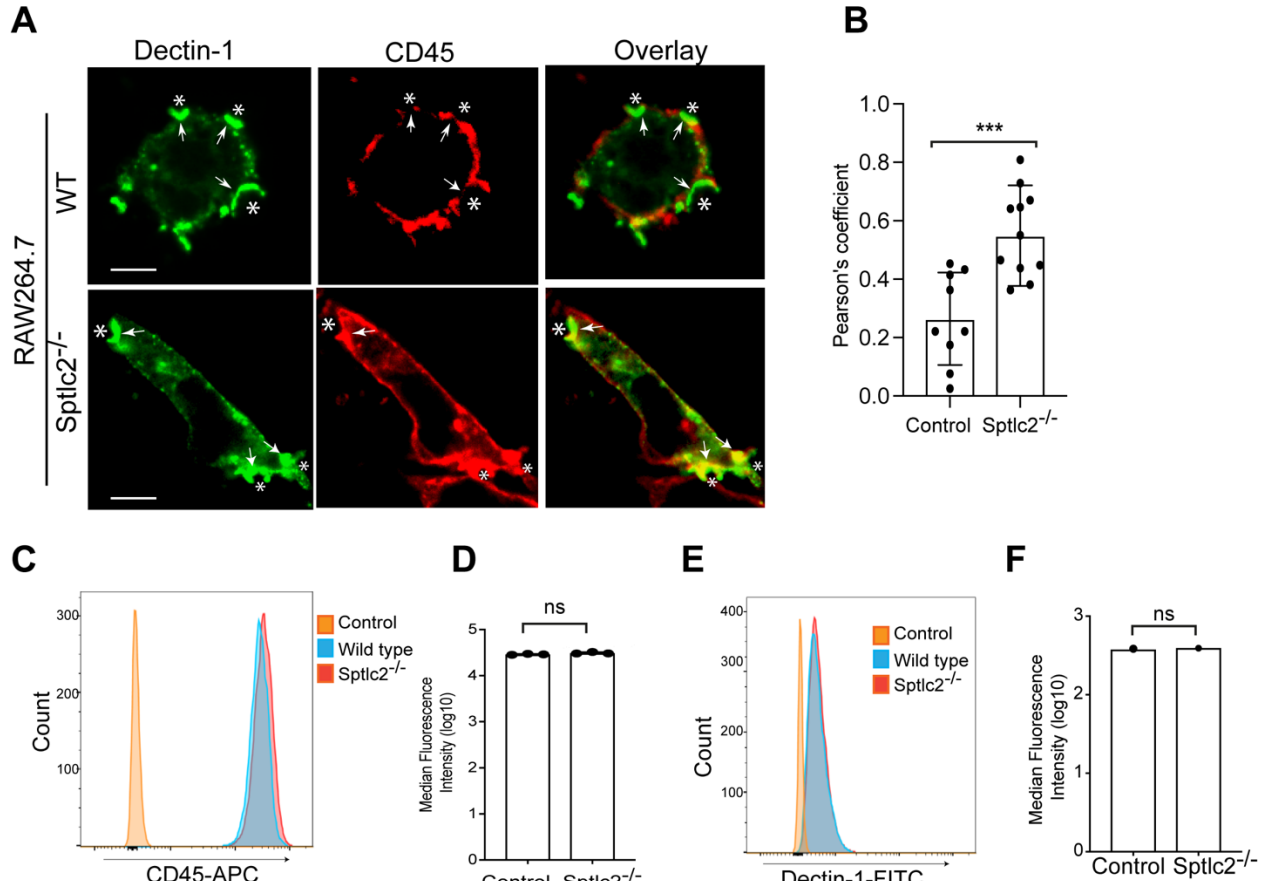


692

693 **Figure 3: Sphingolipid biosynthesis is required for efficient phagocytosis of Mtb and Zymosan A, but**

694 not for HSV entry. (A) Representative images of wildtype and Sptlc2<sup>-/-</sup> RAW 264.7 (A) and DC2.4 (C)  
695 cells infected with mCherry-expressing Mtb. (B, D) Quantification of Mtb uptake for experiments  
696 performed as in A and C, respectively. (E) Representative images of wildtype and Sptlc2<sup>-/-</sup> RAW 264.7 cells  
697 infected with Alexa fluor 594-conjugated Zymosan A particles. (F) Quantification of Zymosan A uptake  
698 uptake performed as in E. (G) Microscopy images of cells that were infected with HSV-mCherry (MOI of  
699 10). At 12 h post infection, cells were fixed, stained with DAPI and analyzed by microscopy. (H)  
700 Quantification of experiments performed as described G. Three independent experiments were performed  
701 each in triplicate with at least 1,000 cells quantified per replicate. Data are mean ± SD. \*\*\*p<0.001, two-  
702 tailed unpaired t-test. Data are mean ± SD. \*\*p<0.01, \*\*\*p<0.001, ns = not significant, two-tailed unpaired  
703 t-test.

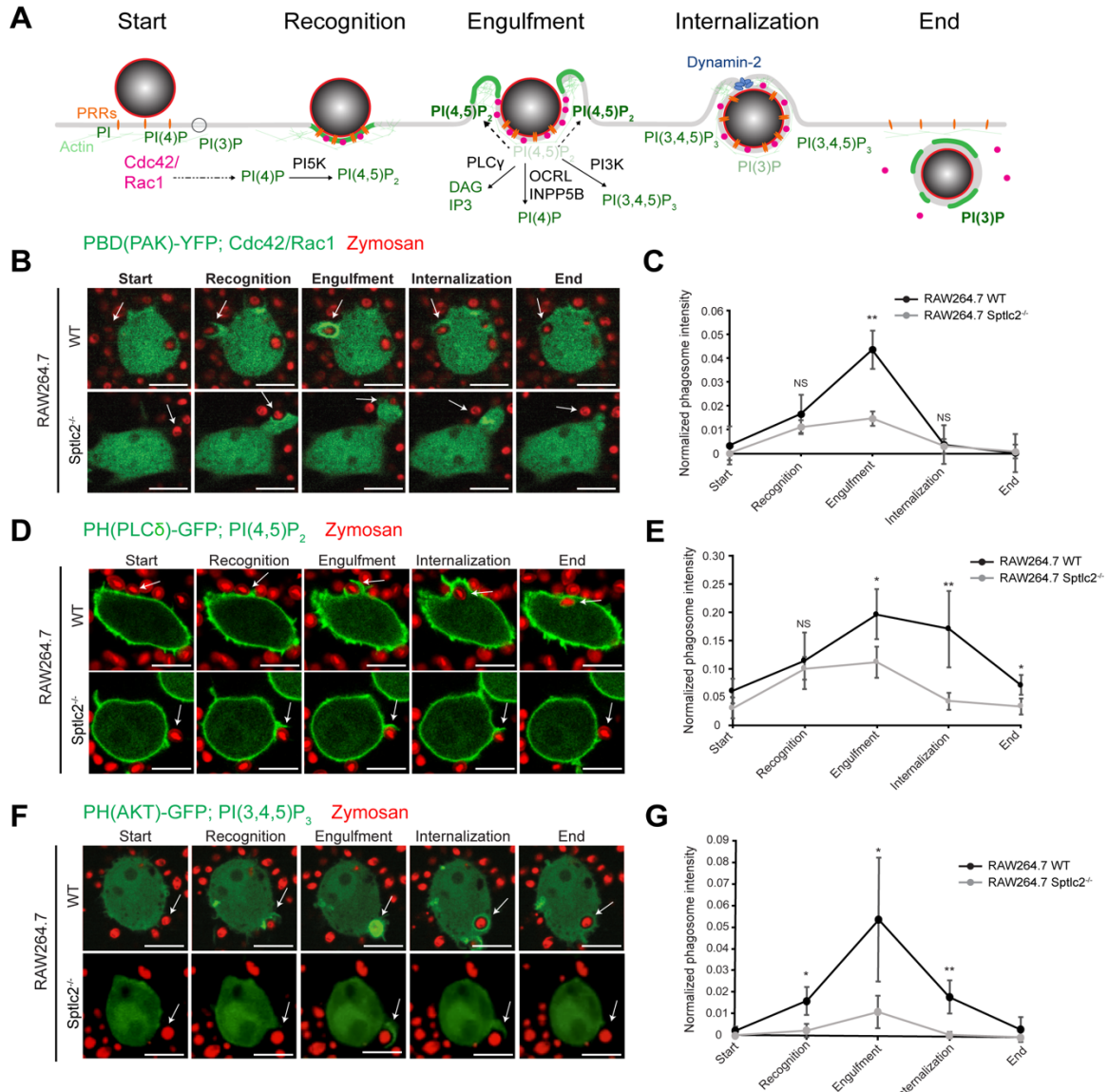
704



705

**Figure 4: Exclusion of CD45 by Dectin-1 from the cup formation site is impaired in Sptlc2<sup>-/-</sup> cells.**  
706 (A) Confocal microscopy of GFP-tagged Dectin-1-expressing RAW264.7 macrophages stimulated with  
707 Zymosan A for 2 min and stained for CD45 (red). Zymosan particles are shown in star (\*) at the  
708 phagocytic cup. (B) Colocalization measurement of CD45 and Dectin-1 at the site of cup formation as  
709 presented by Pearson's colocalization coefficient. (C, E) Flow cytometry of wildtype and Sptlc2<sup>-/-</sup>  
710 RAW264.7 cells that were stained for CD45 and Dectin-1 at the cell surface. (D, F) Graphs showing  
711 quantification of cell surface expression of the receptors described in C and E, respectively. All data are  
712 representative of 3 independent experiments performed in triplicate. Data are mean  $\pm$  SD. ns = not  
713 significant, two-tailed unpaired t-test.  
714

715



716

717 **Figure 5. Sphingolipids are essential for efficient recruitment of Rac1/Cdc42 and phosphoinositide**

718 turnover at the phagocytic cup. (A) Schematic representation of the small GTPase Rac1/Cdc42 and

719 phosphoinositide dynamics during phagocytosis. (B) Confocal images of wild type and Sptlc2<sup>-/-</sup> RAW264.7

720 cells transfected with PAK(PBD)-GFP, a biosensor for active Rac1/Cdc42, during phagocytosis. Cells

721 were incubated with Alexa flour 594-conjugated Zymosan A particles, and live imaging was performed.

722 Images captured at 30-second intervals are shown. (C) A graph showing quantitation of the PAK(PBD)

723 fluorescence intensity in the course of formation of a phagocytic cup (shown in arrow) as performed in B.

724 (D, F) Time-lapse confocal microscopy images of wildtype and Sptlc2<sup>-/-</sup> RAW 264.7 cells expressing

725 PH(PLCδ)-GFP, the PI(4,5)P<sub>2</sub> biosensor (D) or PH(AKT)-GFP, the (PI3,4,5)P<sub>3</sub> biosensor (F) after infection

726 with Alexa flour 594 conjugated Zymosan A particles at MOI of 10. Representative images that are captured

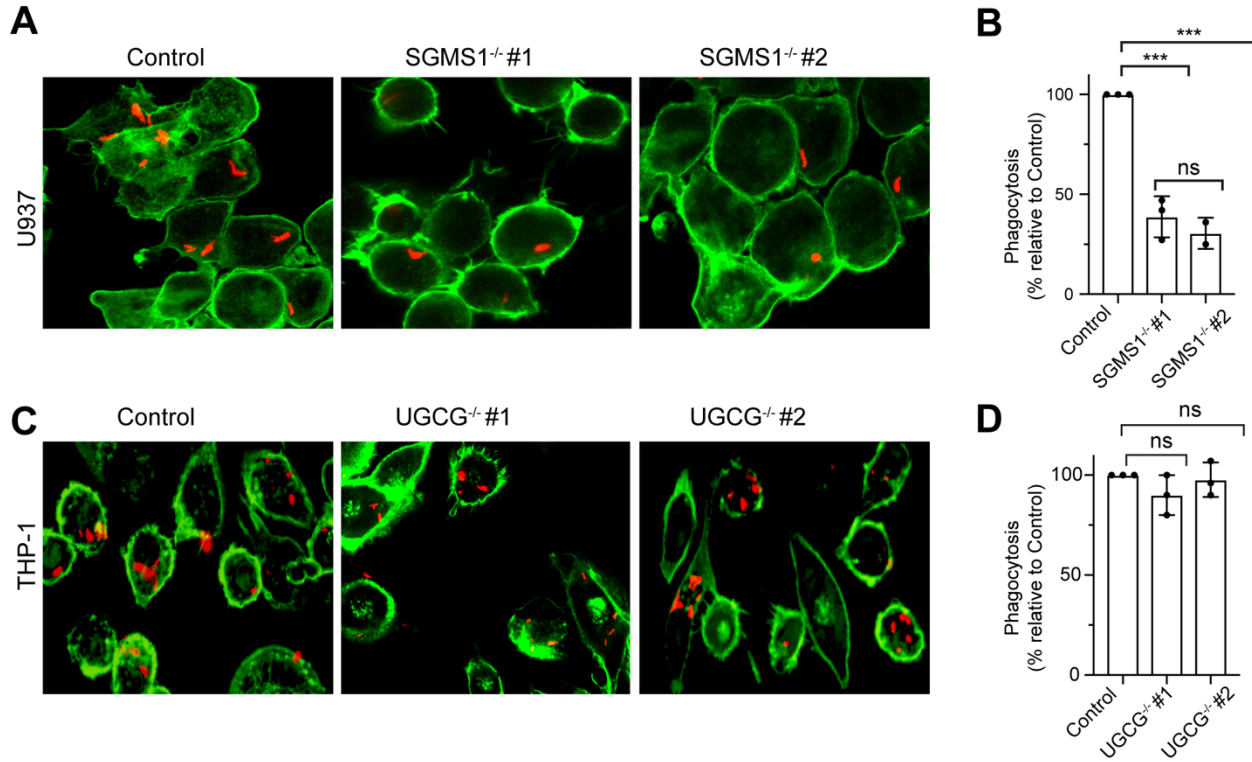
727 at 30-second intervals are shown. (E, G) Accumulation of GFP signal to site of particle binding was

728 quantified by the ratio of GFP signal intensity at phagosome versus GFP signal across entire cell at the

729 indicated time points for experiments performed as D and F. n= 3 independent experiments and the mean

730 GFP intensity profiles of 10 - 20 cells are represented. Data are mean ± SD. \*p<0.05, \*\*p<0.01, two-tailed

731 unpaired t-test, ns = not significant

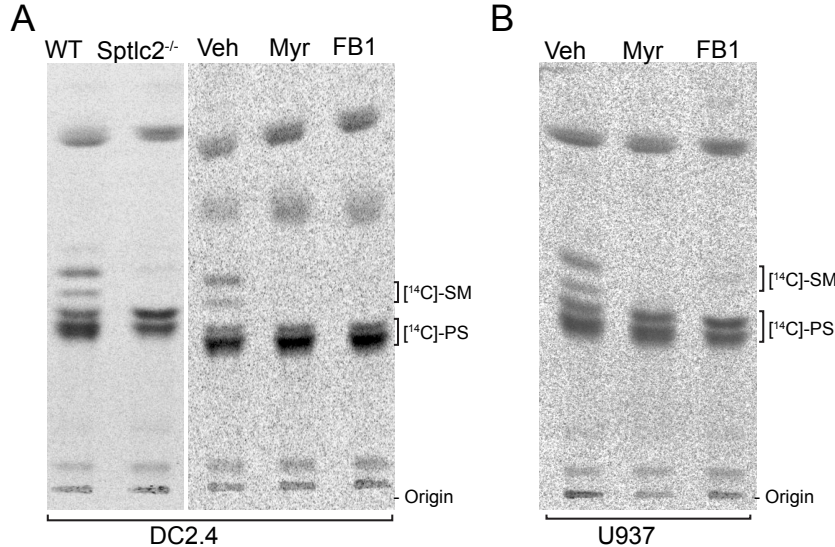


732

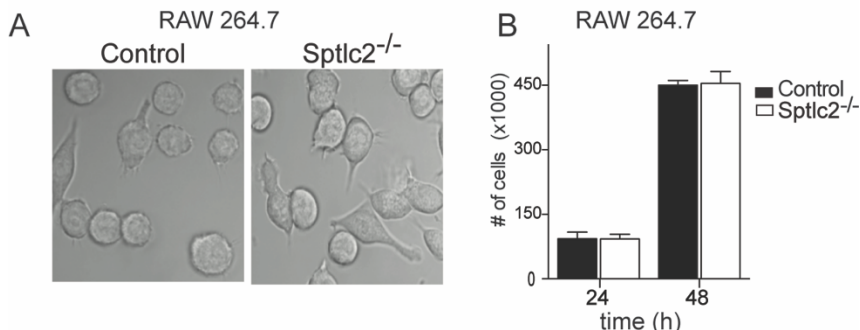
733 **Figure 6: SGMS1<sup>-/-</sup> cells, but not UGCG<sup>-/-</sup>, are defective in phagocytic uptake of Mtb.**

734 (A, C) Representative images of wildtype and two clonal isolates of SGMS1 CRISPR/Cas9 knockout  
735 U937 cells (A) and THP-1 cells deficient in UGCG (Glucosylceramide synthase) gene infected with  
736 mCherry-expressing Mtb. Cells were activated with 80nM PMA for 24 h before Mtb infection. (B, D)  
737 Quantification of Mtb uptake for experiments described as in A and C, respectively. Three independent  
738 experiments were performed each in triplicate with at least 1,000 cells quantified per replicate. Data are  
739 mean  $\pm$  SD. \*\*\*p<0.001, ns = not significant, two-tailed unpaired t-test.

740  
741



742  
743 **Supplemental Figure 1: Genetic and small molecule inhibitors mediated depletion of sphingolipid in**  
744 **phagocytes.** (A, B) Control, mutant and inhibitor-treated cells were labeled with the sphingolipid  
745 precursor 3-L-[<sup>14</sup>C]-serine, and total lipids were extracted and analyzed by thin layer chromatography and  
746 autoradiography. All data are representative of 3 independent experiments.  
747  
748



749  
750 **Supplemental Figure 2: Depletion of sphingolipids has no effect on cell morphology, growth rate or**  
751 **cell division.** (A) Microscopy images of control and Sptlc2<sup>-/-</sup> RAW 264.7 macrophages, showing no  
752 morphological difference between the mutant and control cells. (B) The cell division of the control and  
753 Sptlc2<sup>-/-</sup> RAW 264.7 macrophages at different time points was measured and presented.  
754  
755  
756  
757